

Electric dipole moments and disalignment of interstellar dust grains

Margaret E. Jordan^{*} & Joseph C. Weingartner^{*}

Department of Physics and Astronomy, George Mason University, MSN 3F3, 4400 University Drive, Fairfax, VA 22030, USA

27 October 2021

ABSTRACT

The degree to which interstellar grains align with respect to the interstellar magnetic field depends on disaligning as well as aligning mechanisms. For decades, it was assumed that disalignment was due primarily to the random angular impulses a grain receives when colliding with gas-phase atoms. Recently, a new disalignment mechanism has been considered, which may be very potent for a grain that has a time-varying electric dipole moment and drifts across the magnetic field. We provide quantitative estimates of the disalignment times for silicate grains with size $\gtrsim 0.1\mu\text{m}$. These appear to be shorter than the time-scale for alignment by radiative torques, unless the grains contain superparamagnetic inclusions.

Key words: dust, extinction – ISM: magnetic fields

1 INTRODUCTION

Observations of starlight polarization have revealed that some interstellar dust grains are non-spherical and aligned. The degree of alignment, and hence the polarization, depends on both aligning processes (e.g., radiative torques and paramagnetic dissipation) and disaligning processes (e.g., random torques arising from collisions with gas atoms). See Whittet (2004) for a review of polarization observations and Lazarian (2003), Roberge (2004), and Lazarian (2007) for reviews of alignment theory.

Recently, Weingartner (2006, hereafter W06) proposed an alternative disalignment mechanism for a grain that has a time-varying electric dipole moment \mathbf{p} and drifts across the interstellar magnetic field. The potency of this mechanism is sensitive to the magnitude and time-scale of fluctuations in \mathbf{p} . W06 considered highly simplified models for the fluctuating electric dipole moment. Here, we examine this process and the implications for disalignment in greater detail. We will consider relatively large (size $\gtrsim 0.1\mu\text{m}$) silicate grains, since the 9.7 and 20 μm features exhibit polarization (e.g., Martin & Whittet 1990; Smith et al. 2000; Wright et al. 2002) and the wavelength dependence of the observed polarization implies that relatively small grains are not efficient polarizers (Kim & Martin 1995).

In §2, we review the main elements of disalignment associated with fluctuations in \mathbf{p} . Next, we introduce models for the transport of charge to and within silicate grains (§3). We describe simulations of the fluctuating dipole moment

and associated disalignment in §4 and present results in §5 and conclusions in §6.

2 DISALIGNMENT ASSOCIATED WITH TIME-VARYING ELECTRIC DIPOLE MOMENTS

When a gas atom collides with a grain, it imparts an angular impulse to the grain. If no other mechanisms excite rotation, then the energy in rotation about any axis is $\sim \frac{1}{2}k_{\text{B}}T_{\text{gas}}$, where k_{B} is Boltzmann’s constant and T_{gas} is the gas temperature. Such motion is called ‘thermal rotation’. The thermal rotation rate for a sphere with radius a is given by

$$\begin{aligned}\omega_T &= \left(\frac{15k_{\text{B}}T_{\text{gas}}}{8\pi\rho a^5} \right)^{1/2} \\ &= 1.66 \times 10^5 \left(\frac{\rho}{3\text{ g cm}^{-3}} \right)^{-1/2} \left(\frac{T_{\text{gas}}}{100\text{ K}} \right)^{1/2} \\ &\quad \times \left(\frac{a}{0.1\mu\text{m}} \right)^{-5/2} \text{ s}^{-1},\end{aligned}\tag{1}$$

where ρ is the density of the grain material. In general, grains are subjected to additional torques that may drive them to suprathermal rotation, with angular speed $\omega > \omega_T$ (Purcell 1975, 1979; Draine & Lazarian 1998). For thermally rotating grains, the random collisional impulses constitute an important disalignment mechanism.

A spinning grain with non-zero electric charge acquires a magnetic dipole moment $\boldsymbol{\mu} \parallel \boldsymbol{\omega}$ (Martin 1971). Dolginov

^{*} Email: mjordan4@gmu.edu; jweinga1@gmu.edu

& Mytrophanov (1976) showed that the Barnett effect (i.e., the tendency for a spinning paramagnetic solid to acquire a magnetization parallel or anti-parallel to $\boldsymbol{\omega}$) can provide a much larger moment. Specifically, the Barnett magnetic moment $\boldsymbol{\mu}_{\text{Bar}} = \chi_0 \boldsymbol{\omega} V / \gamma_g$, where χ_0 is the static magnetic susceptibility, γ_g is the gyromagnetic ratio of the microscopic magnetic dipoles that are responsible for the grain's paramagnetism, and V is the grain volume. The susceptibility depends on the number density of paramagnetic ions or nuclei in the grain material and is thus rather uncertain. We will adopt $\chi_0 \sim 5 \times 10^{-3} (T_d/15 \text{ K})^{-1}$, where T_d is the grain temperature (Draine 1996; W06). With this estimate, the Barnett magnetic moment for silicate grains is

$$|\boldsymbol{\mu}_{\text{Bar}}|(\text{sil}) \approx 1.2 \times 10^{-19} \left(\frac{T_d}{15 \text{ K}} \right)^{-1} \left(\frac{a}{0.1 \mu\text{m}} \right)^3 \times \left(\frac{\omega}{10^5 \text{ s}^{-1}} \right) \text{ statC cm.} \quad (2)$$

Suppose $\boldsymbol{\mu}$ is parallel or anti-parallel to the grain's angular momentum vector \boldsymbol{J} : $\boldsymbol{\mu} = \mu_J \hat{\boldsymbol{J}}$. The magnetic torque $\boldsymbol{\Gamma}_\mu = \boldsymbol{\mu} \times \boldsymbol{B}$ causes \boldsymbol{J} to precess about the interstellar magnetic field \boldsymbol{B} at rate

$$|\Omega_0| = \frac{|\boldsymbol{\mu}|B}{J} \approx 314 \left(\frac{|\boldsymbol{\mu}|}{10^{-19} \text{ statC cm}} \right) \left(\frac{\rho}{3 \text{ g cm}^{-3}} \right)^{-1} \times \left(\frac{B}{5 \mu\text{G}} \right) \left(\frac{a}{0.1 \mu\text{m}} \right)^{-5} \left(\frac{\omega}{10^5 \text{ s}^{-1}} \right)^{-1} \text{ yr}^{-1}. \quad (3)$$

Since $\boldsymbol{\mu} \propto \boldsymbol{\omega}$, Ω_0 is independent of ω . The combination of an aligning torque (e.g., the radiative torque) and the magnetic torque drives the grain towards rapid precession with a constant precession angle θ_{align} (i.e., θ_{align} is the angle between \boldsymbol{B} and \boldsymbol{J}). A large ensemble of grains will be characterized by a uniform distribution in precession phase. As a result, the observed starlight polarization is either parallel or perpendicular to \boldsymbol{B} . (If $\theta_{\text{align}} = 0$ and $\boldsymbol{J} \parallel \hat{\boldsymbol{a}}_1$, the grain principal axis of greatest moment of inertia, then the polarization $\parallel \boldsymbol{B}$.) Note that alignment of the grain body with respect to \boldsymbol{J} is also a necessary condition for polarization.

If a grain has an electric dipole moment \boldsymbol{p} and drifts with velocity \boldsymbol{v} across \boldsymbol{B} , then it experiences a torque $\boldsymbol{\Gamma}_p = \boldsymbol{p} \times (\boldsymbol{v} \times \boldsymbol{B})/c$ in addition to the magnetic torque (c is the speed of light). If $\boldsymbol{p} = p_J \hat{\boldsymbol{J}}$, then the grain precesses about an axis tilted at angle $\delta = \tan^{-1} |\Upsilon|$ relative to \boldsymbol{B} and the precession rate is increased by the factor $(1 + \Upsilon^2)^{1/2}$, where

$$\Upsilon \equiv \frac{p_J v_\perp}{\mu_J c} \quad (4)$$

with v_\perp the component of \boldsymbol{v} transverse to \boldsymbol{B} (W06).

If $\boldsymbol{\mu}$ and \boldsymbol{p} are not parallel or anti-parallel to \boldsymbol{J} , then the magnetic and electric torques must be averaged over the extremely rapid grain rotation. The resulting dynamics is identical to that for which \boldsymbol{J} , $\boldsymbol{\mu}$, and \boldsymbol{p} all lie along $\hat{\boldsymbol{a}}_1$, except with the following substitutions in equation (4):

$$\mu_J = \left(\frac{\boldsymbol{\mu}}{\omega} \right) \frac{qJ}{I_1}, \quad (5)$$

$$p_J = \pm (\boldsymbol{p} \cdot \hat{\boldsymbol{a}}_i) f_i(q), \quad (6)$$

with I_i the moment of inertia along $\hat{\boldsymbol{a}}_i$ (W06). Both μ_J and p_J depend on the grain's rotational state through the

parameter $q \equiv 2I_1 E / J^2$ (E is the rotational energy). In equation (6), the $+$ ($-$) sign is selected when $\boldsymbol{J} \cdot \hat{\boldsymbol{a}}_i > 0$ (< 0) and the factor $f_i(q)$ is given in eq. 9 of W06. (The choice of i is also discussed following eq. 9 in W06.) If the Barnett effect is responsible for the magnetic dipole moment, then $(\boldsymbol{\mu}/\omega) = \chi_0 V / \gamma_g$.

If Υ is constant in time, then the only consequence of the electric dipole is to tilt the precession axis relative to the magnetic field direction. However, Υ can vary on relatively short time-scales. W06 discussed two sources of variation: 1. Upon each discrete charging event (e.g., the capture of an electron from the gas or photoejection of an electron), p_J changes. 2. When the grain's rotational state (q and/or flip state) varies, p_J/μ_J varies (eqs. 5 and 6).

Two processes can yield rapid variations in the grain rotational state: 1. Thermal fluctuations, in which energy is exchanged between grain rotation and vibrational modes (Lazarian 1994; Lazarian & Roberge 1997; Lazarian & Draine 1997, 1999a, 1999b; Weingartner 2009). 2. Collisions with gas-phase atoms, which can stick to, reflect from, or evaporate from the surface, perhaps after forming a molecule (Hoang & Lazarian 2009). The efficacy of both of these mechanisms drops off dramatically as the grain rotation becomes suprathermal.

In this paper, we will only consider variations in p_J associated with discrete charging events. We also will assume $q = 1$ in equation (5) and $f_i(q) = 1$ in equation (6), which are good approximations for suprathermally rotating grains. Thus, the analysis presented here is not complete for thermally rotating grains.

Since the charging processes are stochastic processes, Υ varies stochastically, yielding random variations in the precession axis. Each time the precession axis changes direction, the precession angle changes. When these events occur at random precession phases, θ_{align} varies stochastically. In other words, the grain experiences disalignment.

W06 considered a simple scenario in which Υ has constant magnitude but stochastically reverses sign, on time-scale τ_{flip} , finding the following approximations for the disalignment time-scale when τ_{flip} is short or long compared with the precession time-scale:

$$\tau_{\text{dis}} \sim \Upsilon^{-2} |\Omega_0|^{-2} \tau_{\text{flip}}^{-1}, \quad \text{if } \tau_{\text{flip}} \ll |\Omega_0|^{-1} (1 + \Upsilon^2)^{-1/2} \quad (7)$$

$$\tau_{\text{dis}} \sim (1 + \Upsilon^2) \tau_{\text{flip}}, \quad \text{if } \tau_{\text{flip}} \gg |\Omega_0|^{-1} (1 + \Upsilon^2)^{-1/2}. \quad (8)$$

In the following section, we will consider more detailed models for the fluctuating electric dipole moment.

3 GRAIN CHARGING MODELS

A grain charging model that follows the evolution of the electric dipole moment \boldsymbol{p} must treat both the processes that deliver charge to the grain and those that transport charge within the grain. In the cold, neutral, interstellar medium, the dominant charge delivery mechanisms are starlight-induced photoelectric emission and sticking collisions of gas-phase electrons.

3.1 Idealizations for Charge Transport Within a Grain

Bulk, neutral silicates are good insulators, with a full valence band and empty conduction band. Observations of the 9.7 μm band profile indicate that interstellar silicates are predominantly amorphous (Li & Draine 2001; Kemper, Vriend, & Tielens 2004; Li, Zhao, & Li 2007). In amorphous materials, localized energy states ('traps') appear in the tails of the conduction and valence bands. For any realistic interstellar grain, there are also localized states associated with impurity atoms. Electrons and holes can hop from site to site with assistance from a phonon (e.g., Mott & Davis 1971; Blaise 2001), so no grain is perfectly insulating.

The rate at which an electron hops from site i to site j is typically approximated as

$$R_{\text{hop}} = \nu_{\text{ph}} \exp(-2r_{ij}/d_{\psi}) \exp(-W_{i \rightarrow j}/k_{\text{B}}T_{\text{d}}) \quad (9)$$

(Ambegaokar et al. 1971; Mady et al. 2007), where $\nu_{\text{ph}} \sim 10^{13} \text{ s}^{-1}$ is the phonon frequency (Brucato et al. 2002), r_{ij} is the distance between sites i and j , d_{ψ} is the electron localization length, $W_{i \rightarrow j} = \max[E_j - E_i, 0]$, E_i is the electron energy when localized at site i , and T_{d} is the dust temperature.

A completely rigorous treatment of the grain electric dipole moment would include following the charges as they hop among traps. However, this approach is not feasible. First, the quantities appearing in equation (9), namely d_{ψ} and the trap energy distribution, are poorly known. Second, even for tight binding at traps (e.g., $d_{\psi} \approx 2 \text{ \AA}$), there are typically numerous neighboring traps for which the hopping time is orders of magnitude smaller than the time between discrete charging events (which itself is orders of magnitude smaller than the disalignment time). This is true even when a charge is well-localized within the vicinity of a particularly deep trap. Given the large disparity in time-scales, the CPU time for a simulation that follows hopping in detail is prohibitive.

Fortunately, a few simple, plausible idealizations are available and do not strain computational resources. We will consider the following 4 models:

1. A perfect insulator. Each time a charge arrives at the grain (either an electron from the gas or a hole left following photoemission), it remains at its arrival point forever. The full hopping model simplifies to this case when $d_{\psi} \rightarrow 0$, if the typical distance between traps is much less than the grain size. This idealization is also reasonable if (a) the typical distance between *deep* traps is much less than the grain size and (b) the deep traps effectively retain charges in their immediate vicinity. That is, a charge is unlikely to leave the 'sphere of influence' of a deep trap before recombining.

2. A perfect conductor. The excess charge on the grain is completely delocalized. For a homogeneous, spherical grain, the electric dipole moment \mathbf{p} vanishes in this case. For non-spherical shapes, $p \propto Z$, the net charge on the grain (in units of the proton charge). This model is probably not suitable for interstellar grains, since we expect Z to be less than the total number of deep traps in the grain. Still, it is useful to consider this case, to constrain the range of possible outcomes.

3. A conducting grain with deep traps. Some number of deep traps are located at random positions within the

grain. When a charge arrives, it immediately moves to the nearest available trap (either occupying it or recombining with a resident charge of the opposite sign). This model approaches case (1) as the number density of deep traps increases.

4. A partially conducting grain with deep traps. Same as (3), except that a charge executes a random walk through the grain, with some typical step size and frequency, until it comes close to an available deep trap, where it gets stuck. We assume that any adsorbates present on the grain surface are sufficiently dilute that there is no associated enhancement in conductivity along the surface.

3.2 Collisional Charging

The trajectories of charged particles in the vicinity of a grain with non-vanishing electric dipole moment \mathbf{p} differ from those for the $\mathbf{p} = 0$ case. The distribution of arrival sites on the grain surface is such as to reduce $p = |\mathbf{p}|$. Except for model (2) in §3.1, this effect is critical for limiting p . However, it is extremely difficult to treat for non-spherical grain shapes. Thus, we will always treat the grain as a sphere when computing collisional charging rates and the arrival sites of colliding particles. For further simplification in these calculations, we also neglect the motion of the grain with respect to the gas. Even though the grain's speed is assumed to be roughly the sound speed of the gas, the speed of the light electrons is greater by a factor $\approx (m_p/m_e)^{1/2}$ (m_p and m_e are the proton and electron mass, respectively). Thus, we do not expect this assumption to introduce serious error for electron collisional charging. In addition, we neglect ion collisional charging, which is dominated by photoelectric emission. These simplifications are justified in Appendix A.

For a grain at rest with respect to the gas, the collisional charging rate is given by

$$R = \pi a^2 n s \left(\frac{8k_{\text{B}}T_{\text{gas}}}{\pi m} \right)^{1/2} \tilde{R} \quad (10)$$

where n is the number density of the colliding particles, s is the sticking coefficient (i.e., the probability that the particle sticks to the grain following a collision), m is the mass of colliding particle, and \tilde{R} accounts for deviations of the collision cross section from the geometric cross section. For the relatively large grains under consideration here, we adopt $s \approx 1/2$ (Weingartner & Draine 2001, hereafter WD01). Draine & Sutin (1987) provided expressions for \tilde{R} for a charged, conducting sphere, including the polarization of the grain by the charged gas-phase particle. The effect of polarization decreases with grain size (as long as T_{gas} does not approach zero), and can be reasonably neglected when $a \geq 0.1 \mu\text{m}$.

Consider a spherical grain with radius a centered at the origin. Approximate the charge distribution within the grain as a point charge Q and point dipole $p\hat{\mathbf{z}}$ ($p > 0$) located at the origin. In spherical coordinates (r, θ, ϕ) , the electric force on a point charge q is

$$\mathbf{F} = \frac{Qq}{r^2} \hat{\mathbf{r}} + \frac{qp}{r^3} (2 \cos \theta \hat{\mathbf{r}} + \sin \theta \hat{\boldsymbol{\theta}}) \quad (11)$$

and the potential is

$$U = \frac{Qq}{r} + \frac{qp \cos \theta}{r^2}. \quad (12)$$

The equations of motion are

$$m\ddot{r} = m\dot{r}\dot{\theta}^2 + mr\sin^2\theta\dot{\phi}^2 + \frac{Qq}{r^2} + \frac{2qp\cos\theta}{r^3} \quad (13)$$

$$mr\ddot{\theta} = -2m\dot{r}\dot{\theta} + mr\sin\theta\cos\theta\dot{\phi}^2 + \frac{qp\sin\theta}{r^3} \quad (14)$$

$$mr\sin\theta\ddot{\phi} = -2m\dot{r}\sin\theta\dot{\phi} - 2mr\cos\theta\dot{\theta}\dot{\phi} \quad (15)$$

where dots denote differentiation with respect to time and m is the mass of the point charge q .

Employing Hamilton-Jacobi theory, we find the following conserved quantities:

$$p_\phi \equiv mr^2\sin^2\theta\dot{\phi} \quad (16)$$

$$\beta \equiv m^2r^4\dot{\theta}^2 + 2mqp\cos\theta + \frac{p_\phi^2}{\sin^2\theta} \quad (17)$$

$$E \equiv \frac{1}{2}m\dot{r}^2 + \frac{Qq}{r} + \frac{\beta}{2mr^2}, \quad (18)$$

as can be verified by direct time differentiation, substituting for the second derivatives from equations (13)–(15).

Our goals are to find (1) the rate at which incoming charged particles strike the grain surface and (2) the distribution of their arrival angles θ , given Q , p and T_{gas} . First, we describe the trajectory of the incoming particle when it is still far from the grain (see Fig. 1). Suppose its velocity is

$$\mathbf{v}_\infty = -v(\cos\theta_0\hat{\mathbf{z}} + \sin\theta_0\hat{\mathbf{x}}). \quad (19)$$

The trajectory is offset from the line $x = \tan\theta_0 z$, which passes through the grain center, by impact parameter b ; angle α specifies the displacement of the trajectory from the $x-z$ plane. Consider a plane front of incoming particles. When the particle whose trajectory passes through the origin is located at distance r_0 from the origin, the coordinates of the other particles are

$$(r, \theta, \phi) \approx \left(r_0, \theta_0 + \cos\alpha\frac{b}{r_0}, \frac{\sin\alpha}{\sin\theta_0}\frac{b}{r_0} \right) \quad (20)$$

and the components of their velocities are

$$\dot{r} \approx -v \quad (21)$$

$$r\dot{\theta} \approx v\cos\alpha(b/r_0) \quad (22)$$

$$r\sin\theta\dot{\phi} \approx v\sin\alpha(b/r_0). \quad (23)$$

Expressing the time derivatives in equations (16)–(18) using equations (21)–(23) yields

$$p_\phi = mvb\sin\theta_0\sin\alpha \quad (24)$$

$$\beta = m^2v^2b^2 + 2mqp\cos\theta_0 \quad (25)$$

$$E = mv^2/2. \quad (26)$$

Substituting these results in equations (17) and (18), we find

$$\dot{r}^2 = v^2\left(1 - \frac{b^2}{r^2}\right) - \frac{2q}{mr}\left(Q + \frac{p\cos\theta_0}{r}\right) \quad (27)$$

$$r^4\dot{\theta}^2 = v^2b^2\left(1 - \frac{\sin^2\theta_0\sin^2\alpha}{\sin^2\theta}\right) + \frac{2qp}{m}(\cos\theta_0 - \cos\theta). \quad (28)$$

We are interested in the solution with $\dot{r} < 0$, since the particle approaches the grain. The choice of the initial sign S is more complicated for $\dot{\theta}$. If $\theta_0 = 0$ (π), then $S = +1$ ($S = -1$). Otherwise, equation (22) yields $\dot{\theta} = vb\cos\alpha/r^2$

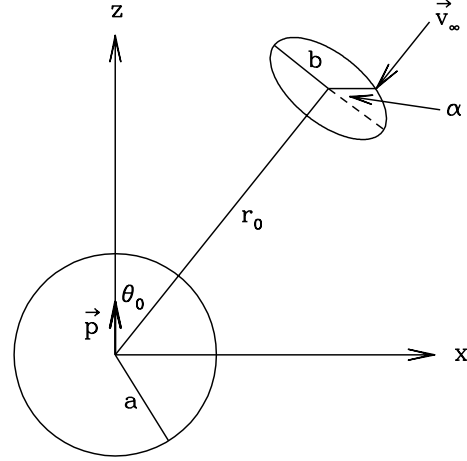


Figure 1. Parameters describing the trajectories of incoming charged particles.

for $r \rightarrow \infty$. Thus, $S = +1$ ($S = -1$) when $\cos\alpha > 0$ ($\cos\alpha < 0$). When $\cos\alpha = 0$, it is necessary to consider the second order term in the expansion for $\dot{\theta}$: $\sin\theta r\dot{\theta} = v\cos\theta_0(b/r_0)^2$. Thus, in this case, $S = \cos\theta_0/|\cos\theta_0|$. If $\cos\theta_0$ and $\cos\alpha$ both equal zero, then $\dot{\theta} \equiv 0$. Note that S typically changes sign at points θ where $\dot{\theta} = 0$.

Since \dot{r}^2 is a single-valued function of r (eq. 27), charge q only reaches the grain surface if \dot{r} does not reverse sign when $r > a$. From equation (27), $\dot{r} = 0$ when

$$r = a \left[U \pm \sqrt{U^2 + V\cos\theta_0 + \left(\frac{b}{a}\right)^2} \right] \quad (29)$$

where $U \equiv qQ/(mv^2a)$ and $V \equiv 2qp/(mv^2a^2)$. If the larger root in equation (29), r_+ , exceeds a and $\dot{r} > 0$ at $r = r_+$, then charge q does not strike the grain. If $U > 1$, then charge q only strikes the grain if the argument of the square root in equation (29) is negative, since \dot{r} never reaches zero in this case. Assuming $\dot{r} > 0$ at r_+ , the critical impact parameter is given by

$$\frac{b_{\text{crit}}}{a} = \begin{cases} (1 - 2U - V\cos\theta_0)^{1/2}, & U \leq 1 \\ (-U^2 - V\cos\theta_0)^{1/2}, & U \geq 1 \end{cases} \quad (30)$$

Only trajectories with $b \leq b_{\text{crit}}$ strike the grain surface. If the relevant root in equation (30) is not real, then $b_{\text{crit}} = 0$. Note that b_{crit} does not depend on the angle α . The collision cross section is πb_{crit}^2 .

Now we justify the assumption that $\dot{r} > 0$ at $r = r_+$ when $b = b_{\text{crit}}$. Differentiating equation (18) yields

$$\dot{r} \left(\ddot{r} - \frac{qQ}{mr^2} - \frac{\beta}{m^2r^3} \right) = 0. \quad (31)$$

The term in parentheses in equation (31) must vanish for all r , except where $\dot{r} = 0$. Continuity implies that it vanishes at these locations as well, including at $r = r_+$. Equations (29) and (31) yield

$$\ddot{r} = \frac{a^2 v^2}{r_+^3} \left[U^2 + V \cos \theta_0 + \left(\frac{b}{a} \right)^2 + U \sqrt{U^2 + V \cos \theta_0 + \left(\frac{b}{a} \right)^2} \right] \quad (32)$$

at $r = r_+$. If either $U > 0$ or $V \cos \theta_0 > 0$, then clearly $\ddot{r} > 0$ at $r = r_+$, regardless of b . If both of these quantities are negative, then setting $b = b_{\text{crit}}$ in equation (32) yields $\ddot{r} = |U - 1| > 0$ for $r = r_+$.

Assuming no gas-grain drift, the mean collision cross section (averaged over angle θ_0) is

$$\bar{\sigma} = \begin{cases} \pi a^2 (1 - 2U) & , 2U + |V| \leq 1 \\ 0 & , 2U - |V| \geq 1 \\ \frac{1}{4} \pi a^2 |V|^{-1} (1 - 2U + |V|)^2 & , \text{otherwise} \end{cases} \quad (33)$$

when $U \leq 1$ and

$$\bar{\sigma} = \begin{cases} \frac{1}{4} \pi a^2 |V| (1 - |V|^{-1} U^2)^2 & , |V|^{-1} U^2 < 1 \\ 0 & , |V|^{-1} U^2 \geq 1 \end{cases} \quad (34)$$

when $U \geq 1$.

Integrating over the Maxwell speed distribution yields the factor \tilde{R} from equation (10) for a grain that does not drift relative to the gas:

$$\tilde{R}(\gamma, |\eta|) = 1 - \gamma, \quad qQ < 0 \quad \text{and} \quad |\eta| \leq -\gamma \quad (35)$$

$$\tilde{R} = \frac{1}{4|\eta|} \left\{ (|\eta| - \gamma)(2 + |\eta| - \gamma) + 2 \left[1 - e^{-(\gamma+|\eta|)} \right] \right\}, \quad qQ < 0 \quad \text{and} \quad |\eta| \geq -\gamma \quad (36)$$

$$\tilde{R} = e^{-\gamma} \frac{\sinh |\eta|}{|\eta|}, \quad qQ > 0 \quad \text{and} \quad |\eta| \leq \gamma/2 \quad (37)$$

$$\begin{aligned} \tilde{R} &= -\frac{1}{2|\eta|} e^{-(\gamma+|\eta|)} \\ &+ \frac{|\eta|^2 + (2-\gamma)|\eta| + (2-\gamma + \gamma^2/4)}{4|\eta|} e^{-\gamma/2} \\ &+ \frac{|\eta|}{4} \int_{\gamma^2/(4|\eta|)}^{\gamma/2} ds \left(1 - \frac{\gamma^2}{4|\eta|s} \right)^2 e^{-s}, \\ &qQ > 0 \quad \text{and} \quad |\eta| \geq \gamma/2; \end{aligned} \quad (38)$$

$\gamma \equiv qQ/(ak_B T_{\text{gas}})$, and $\eta \equiv qp/(a^2 k_B T_{\text{gas}})$. Fig. 2 displays \tilde{R} versus γ for various values of $|\eta|$. Note that equations (35) and (37) recover the classic Spitzer (1941) expression for \tilde{R} for a charged sphere when $\eta = 0$.

Since $d\theta/dr = \dot{\theta}/\dot{r}$, equations (27) and (28) yield

$$F_1(\theta_0, \theta, VC^2, \alpha) = F_2(A, B, C) \quad (39)$$

where

$$A \equiv 1 + VC^2 \cos \theta_0 \quad (40)$$

$$B \equiv 2UC \quad (41)$$

$$C \equiv a/b \quad (42)$$

$$F_1(\theta_0, \theta, VC^2, \alpha) = \quad (43)$$

$$\int_{\theta_0}^{\theta} \frac{|\sin \theta'| d\theta' S(\theta')}{\sqrt{\sin^2 \theta' - \sin^2 \theta_0 \sin^2 \alpha + VC^2 \sin^2 \theta' (\cos \theta_0 - \cos \theta')}} \quad (44)$$

$$F_2(A, B, C) = \int_C^{\infty} \frac{du}{u\sqrt{-A - Bu + u^2}}. \quad (44)$$

The integrand in equation (43) is negative when $S < 0$, but in these cases $\theta < \theta_0$, so the integral remains positive.

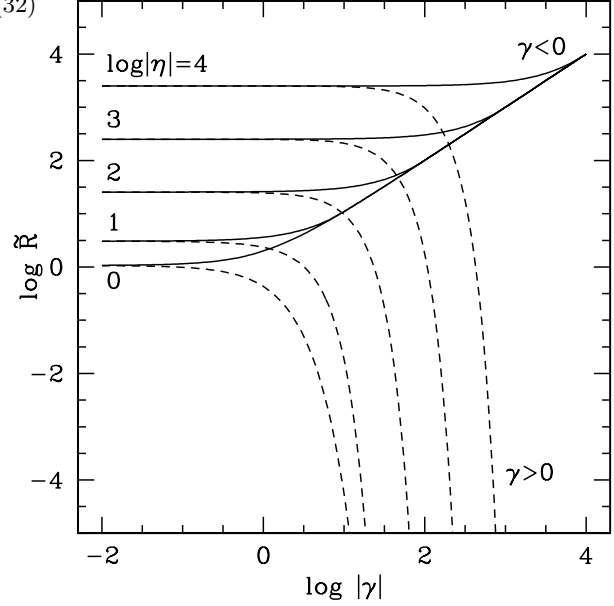


Figure 2. \tilde{R} vs. γ for various values of $|\eta|$, as indicated.

If $\dot{\theta}$ reaches zero at $\theta' = \theta_1$, then S changes sign and F_1 splits into two integrals, with limits θ_0 to θ_1 and θ_1 to θ . Performing the integration in equation (44),

$$F_2 = \frac{1}{\sqrt{A}} \left[\sin^{-1} \left(\frac{BC + 2A}{C\sqrt{B^2 + 4A}} \right) - \sin^{-1} \left(\frac{B}{\sqrt{B^2 + 4A}} \right) \right], \quad A \geq 0 \quad (45)$$

$$F_2 = \frac{1}{\sqrt{-A}} \ln \left[\frac{2\sqrt{-A}\sqrt{C^2 - BC - A} - BC - 2A}{(2\sqrt{-A} - B)C} \right], \quad A \leq 0. \quad (46)$$

Given $2qp/(mv^2 b^2)$, $2qQ/(mv^2 b)$, a/b , θ_0 , and α , equation (39) can be solved to efficiently find the arrival angle θ . A less efficient, but more direct, approach is to integrate the equations of motion (13)–(15). We have written FORTRAN subroutines implementing both of these methods and found perfect agreement for numerous combinations of input parameters.

To compute the distribution of arrival angles θ for given values of γ and η , we examine a large number of trajectories with initial parameters θ_0 , $u \equiv v/v_{\text{th}}$, b/a , and α , where $v_{\text{th}} \equiv (2k_B T_{\text{gas}}/m)^{1/2}$. We first select N_θ values of θ_0 from 0 to π , uniformly spaced in $\cos \theta_0$. For each value of θ_0 , we select N_u values of u , starting with $u = 1.08765$, the median value assuming the Maxwell speed distribution. We then select $(N_u - 1)/2$ values with $u > 1.08765$ spaced in equal-probability intervals, i.e., such that

$$\frac{4}{\sqrt{\pi}} \int_{u_i}^{u_{i+1}} du u^2 \exp(-u^2) = \frac{1}{N_u + 1}. \quad (47)$$

Likewise for values with $u < 1.08765$. For each (θ_0, u) pair, if $b_{\text{crit}} > 0$, then we next select N_b values of b/a between 0 and b_{crit}/a , uniformly spaced in b^2 . Finally, for each $(\theta_0, u, b/a)$, we select N_α values of α , uniformly spaced between 0 and 2π . For each trajectory, we compute the arrival angle θ . The

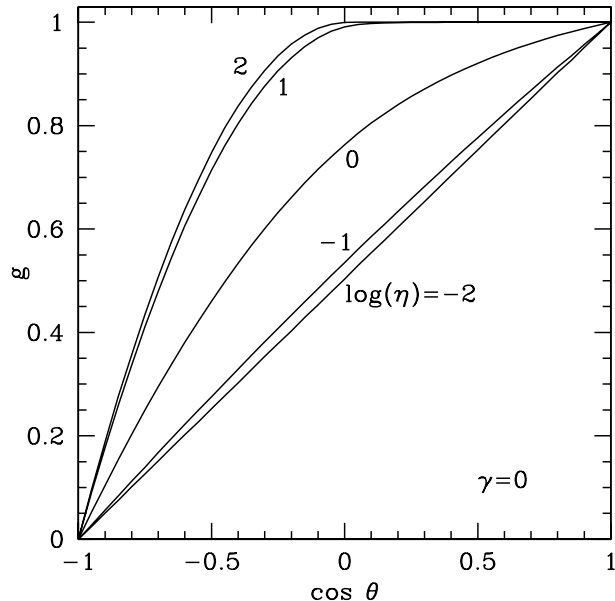


Figure 3. $g(\cos \theta)$ vs. $\cos \theta$ for $\gamma = 0$ and various values of η , as indicated.

results are binned, with trajectories weighted in proportion to b_{crit}^2 .

Fig. 3 displays $g(\cos \theta)$, the fraction of arriving particles that strike with cosine of the polar angle (relative to the dipole moment) $\leq \cos \theta$, for $\gamma = 0$ and several values of η . To construct this figure, we adopted 40 bins in θ and $N_\theta = N_v = N_b = N_\alpha = 31$. The distributions look very similar to those in fig. 3 when $|\gamma| < 1$. Distributions for $(\gamma, -\eta)$ are identical to those for (γ, η) , except that they are referenced to $\cos \theta = 1$ rather than -1 . That is, $g(\gamma, -\eta; \cos \theta) = g(\gamma, \eta; -\cos \theta)$, with $g(\cos \theta)$ the fraction of particles that strike with cosine of polar angle $\geq \cos \theta$ when $\eta < 0$. As $|\gamma|$ increases, the distribution in $\cos \theta$ becomes more uniform, as seen in Fig. 4 for the case that $\eta = 10^2$.

Electrons arriving at the grain surface can penetrate to within the bulk of the grain, with an e-folding length $l_e \sim 10 \text{ \AA}$ (see paragraph following eq. 13 in WD01). We neglect this penetration since $l_e \ll a$; i.e., all arriving electrons are assumed to be located at $r = a$.

3.3 Photoelectric Emission

We adopt a simplified version of the procedure in WD01 for calculating the rate at which photoelectrons are ejected from the grain, J_{pe} . WD01 express the photoelectric yield (i.e., the probability that an electron is ejected following the absorption of a photon) as a product of three factors: the bulk yield y_0 , a size-dependent yield enhancement factor y_1 , and a term y_2 that accounts for the attraction of ‘attempting’ photoelectrons back to the grain when $Z \geq 0$. (Recall that the grain charge $Q = Ze$, with e the proton charge.) For the relatively large grains under consideration here, $y_1 = 1$. The term y_2 is given by (WD01, eq. 11)

$$y_2 = \begin{cases} E_{\text{high}}^2(E_{\text{high}} - 3E_{\text{low}})/(E_{\text{high}} - E_{\text{low}})^3 & , Z \geq 0 \\ 1 & , Z < 0 \end{cases}, \quad (48)$$

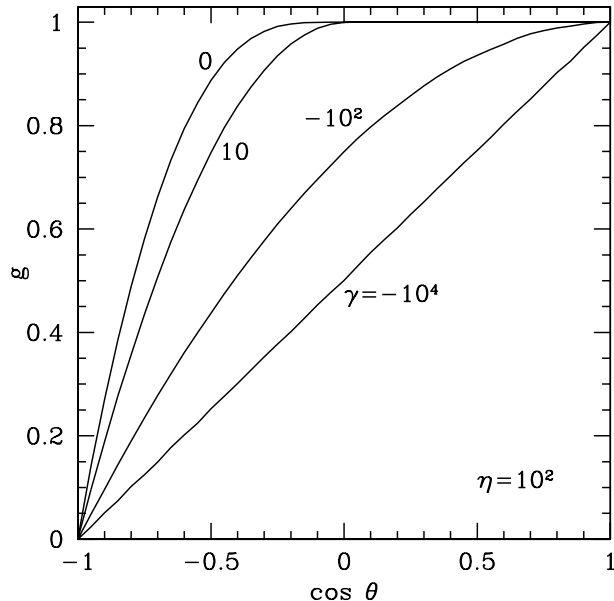


Figure 4. $g(\cos \theta)$ vs. $\cos \theta$ for $\eta = 10^2$ and various values of γ , as indicated.

with $E_{\text{low}} = -(Z + 1)e^2/a$ and $E_{\text{high}} = h\nu - h\nu_{\text{pet}}$ ($h\nu_{\text{pet}}$ is the threshold photon energy for photoemission). For simplicity, we take $E_{\text{high}} = 3 \text{ eV}$ [assuming $h\nu \approx 11 \text{ eV}$ and $h\nu_{\text{pet}} \approx 8 \text{ eV}$ (WD01)], independent of Z and $h\nu_{\text{pet}}$.

To find J_{pe} , it is necessary to integrate the photon absorption rate R_γ times the yield over the range of available photon energies above $h\nu_{\text{pet}}$. Since we approximate y_2 to be independent of $h\nu$, $J_{\text{pe}} \propto y_2$. We simply choose the proportionality constant so as to reproduce the average grain potential of $\approx 0.3 \text{ V}$ from WD01.

As for arriving electrons, we assume that holes produced in photoemission events are located at $r = a$. We also neglect the production of an electron-hole pair when a photon is absorbed but a photoelectron does not escape the grain. In some cases, the photon absorption occurs too deep within the grain for the photoelectron to reach the surface or the photoelectron’s velocity is directed away from the surface (resulting in $y_0 < 1$). Since $l_e \ll a$, the resulting separation of charge does not contribute significantly to the dipole moment. In other cases, a photoelectron breaches the grain surface, but returns to the grain due to an attractive Coulomb force if $Z \geq 0$ (resulting in $y_2 < 1$). Such events could lead to a more significant change in \mathbf{p} , but are rare; $y_2 \approx 0.98$ when the grain potential is 0.3 V .

4 SIMULATIONS

For each of the four charge transport models described in §3.1, we run stochastic simulations that keep track of the grain dipole moment \mathbf{p} and the orientation in space of the grain’s rotational axis, assumed fixed with respect to the grain body (as would be appropriate for suprathermally rotating grains). We adopt $v_\perp = 1 \text{ km s}^{-1}$ (resulting from acceleration associated with magnetohydrodynamic turbulence; Yan et al. 2004), $T_{\text{gas}} = 100 \text{ K}$, $n_e = 4.5 \times 10^{-2} \text{ cm}^{-3}$,

$s_e = 0.5$, $T_d = 15$ K (hence, $\chi_0 = 5 \times 10^{-3}$), and $y_0 = 6 \times 10^{-2}$ (eq. 17 in WD01 with $h\nu = 10$ eV). We consider grains with $a = 0.1$ and $0.2 \mu\text{m}$, for which the photon absorption rate $R_\gamma = 2.9 \times 10^{-2}$ and $5.7 \times 10^{-2} \text{ s}^{-1}$, respectively, in order to maintain the average potential at 0.3 V. We employ a constant time step size dt , usually 31.56 s, which is smaller than the typical time between charging events.

Next, we describe the simulation algorithm for perfectly insulating grains. At the start of each time step, we find the factor \tilde{R} (eq. 10) for the electron collisional charging rate by bilinear interpolation (Press et al. 1992, p. 117) in $\ln \gamma$ and $\ln \eta$, with 21 values of η ranging from 10^{-2} to 10^2 and 11 values of $|\gamma|$ ranging from 10^{-2} to 3×10^2 (for 23 total values of γ in the tables, since both signs, as well as $\gamma = 0$, are included). If $|\gamma| < 10^{-2}$, then a linear interpolation is performed in η alone (with $\gamma = 0$). If $\eta < 10^{-2}$, then we assume the classic Spitzer (1941) expression for \tilde{R} for a charged sphere (corresponding to $\eta = 0$).

An electron arrives with probability $R_e dt$ (R_e is the electron arrival rate; eq. 10). In each time-step, we check that $R_e dt < 1$ (and likewise for the probability that a photoelectron is ejected). Here, as throughout the simulations, we use the routine RAN2 from Press et al. (1992) for choosing random numbers. If $\eta < 10^{-2}$, then the electron is placed at a random location (θ, ϕ) on the grain surface; θ and ϕ are the polar and azimuthal angles, respectively, with the rotation axis $\hat{\omega} = \hat{z}$ as the polar axis. Otherwise, we interpolate to find the distribution function $g(\theta')$, as described in the preceding paragraph for \tilde{R} ; θ' is the polar angle with the dipole moment \mathbf{p} as the polar axis. We choose θ' randomly from the distribution $g(\theta')$ and the azimuthal angle ϕ' is chosen randomly from a uniform distribution. The arrival position with respect to the grain body is given by

$$\begin{aligned}
 x/a &= \sin \theta' (\cos \phi' \cos \theta_p \cos \phi_p - \sin \phi' \sin \phi_p) \\
 &\quad + \cos \theta' \sin \theta_p \cos \phi_p
 \end{aligned} \tag{49}$$

$$\begin{aligned}
 y/a &= \sin \theta' (\cos \phi' \cos \theta_p \sin \phi_p + \sin \phi' \cos \phi_p) \\
 &\quad + \cos \theta' \sin \theta_p \sin \phi_p
 \end{aligned} \tag{50}$$

$$z/a = \cos \theta' \cos \theta_p - \sin \theta' \cos \phi' \sin \theta_p \tag{51}$$

where θ_p and ϕ_p are the polar and azimuthal angles, respectively, of \mathbf{p} relative to the grain body.

A photoelectron is ejected with probability $R_\gamma y_0 y_2$. The resulting hole is located randomly on the grain surface.

At the start of a simulation, we set $\mathbf{p} = 0$ and choose Z to correspond to the average potential of 0.3 V. Draine & Lazarian (1998) noted that a grain may have an intrinsic electric dipole moment due to the random orientations of polar constituents. Thus, our choice $\mathbf{p} = 0$ requires justification.

Consider a conducting grain with N_{dt} deep traps (model 3 in §3.1). The largest possible magnitude of the electric dipole moment associated with excess charges (electrons and holes) occupying the deep traps is $p_{\text{max}} \sim N_{\text{dt}} ea$. If the magnitude of the intrinsic electric dipole moment $p_{\text{int}} > p_{\text{max}}$, then the intrinsic dipole could not be neutralized; thus, flipping of \mathbf{p} would not be possible. This situation is similar to that of a purely conducting grain (model 2 in §3.1) in the cold neutral medium, for which $p \propto Z$ and Z is always positive.

To estimate the likely magnitude of p/ea associated

with the intrinsic dipole, suppose each polar constituent has volume V_0 and dipole moment $p_0 = \zeta eV_0^{1/3}$. Assuming each constituent is randomly oriented, the total intrinsic moment $p_{\text{int}} \sim N^{1/2} p_0$, with the grain volume $(4/3)\pi a^3 = NV_0$. Eliminating N , we find

$$\frac{p_{\text{int}}}{ea} \sim \left(\frac{4\pi}{3}\right)^{1/2} \zeta \left(\frac{a}{V_0^{1/3}}\right)^{1/2}. \tag{52}$$

Even adopting relatively large values of $\zeta \sim 0.1$ and $aV_0^{-1/3} \sim 500$, we find $p_{\text{int}}/ea \sim 4.6$, comparable (in order of magnitude) to the values found in the following section, where the intrinsic electric dipole moment \mathbf{p}_{int} is neglected.

For any realistic grain, $N_{\text{dt}} \gg p_{\text{int}}/ea$; thus, we do not expect the intrinsic electric dipole moment to play any role in the long-term evolution of \mathbf{p} , including the flipping of the dipole moment. Essentially, the total number of charges in the grain (the number of electrons plus the number of holes) can vastly exceed the net number of charges (number of electrons minus number of holes), and a slight asymmetry in the distribution of these charges can counter the intrinsic dipole moment.

Of all the simulations with deep traps considered in this paper, the smallest value of N_{dt} is ≈ 100 , when $a = 0.1 \mu\text{m}$ and the volume per deep trap is $V_t = 4 \times 10^7 \text{ \AA}^3$. (This value of N_{dt} is almost certainly much too small to be realistic, but was chosen to make the computations feasible and to, conservatively, generate a grain with low insulating capability). We ran this model 3 simulation with $p_{\text{int}} = 0$ and with p_{int} as estimated above; the resulting flipping times are nearly identical, as expected.

At any time, the net charge and dipole moment are given by

$$Z = N_h - N_e \tag{53}$$

$$\mathbf{p} = e \sum_{i=1}^{N_h} \mathbf{x}_i - e \sum_{i=1}^{N_e} \mathbf{x}_i \tag{54}$$

where N_h and N_e are the total number of holes and electrons, respectively, and \mathbf{x}_i is the position of an electron or hole (with the origin at the grain's center of mass, i.e., the center of the spherical grain). In each time-step, θ_p , ϕ_p and $p \equiv |\mathbf{p}|$ are updated, if an electron arrives at or departs the grain. We also keep track of θ_{align} and ϕ_{align} , the polar and azimuthal angles of the grain rotation axis with respect to the magnetic field direction, employing eqs. 14 and 15 from W06:

$$d\phi_{\text{align}} = \Omega_0 [1 - \Upsilon \cot \theta_{\text{align}} \cos(\phi_{\text{align}} + \phi_{\text{gyro}})] dt \tag{55}$$

$$d\theta_{\text{align}} = -\Omega_0 \Upsilon \sin(\phi_{\text{align}} + \phi_{\text{gyro}}) dt \tag{56}$$

where Ω_0 is the precession rate for the case that $\mathbf{p} = 0$ (eq. 3),

$$\phi_{\text{gyro}}(t) = \int_0^t dt' \omega_{\text{gyro}}(t'), \tag{57}$$

and the time-scale for gyrorotation is given by

$$\begin{aligned}
 \omega_{\text{gyro}}^{-1} &\sim 2.4 \times 10^2 \left(\frac{\rho}{3 \text{ g cm}^{-3}}\right) \left(\frac{a}{0.1 \mu\text{m}}\right)^2 \left(\frac{U}{0.3 \text{ V}}\right)^{-1} \\
 &\quad \times \left(\frac{B}{5 \mu\text{G}}\right)^{-1} \text{ yr}.
 \end{aligned} \tag{58}$$

Note that ω_{gyro} varies with time, since the grain potential U is not constant.

We take $\theta_{\text{align}} = 0.1$ and $\phi_{\text{align}} = 0$ initially. Within the same charging simulation, we consider several different values of ω/ω_T (and thus, several different values of Υ ; recall eqs. 1, 2, and 4). In principle, gyrorotation can affect the disalignment, since ω_{gyro} fluctuates randomly as Z does so. However, we have found that the disalignment time is identical for simulations that do (do not) include gyrorotation. Thus, we omit gyrorotation in our simulations.

The simulations for purely conducting grains are identical to those for purely insulating grains, except that it is not necessary to keep track of the electron arrival locations, since charge is immediately delocalized. Instead, we simply take $\mathbf{p} = p_z \hat{\mathbf{z}} \propto Z$.

For the models containing deep traps, we first specify the average grain volume per deep trap of a given type (i.e., a trap that accomodates electrons versus one that accomodates holes), V_t , then randomly place $\text{int}(4\pi a^3/3V_t)$ deep traps of each type throughout the grain volume. For model 3 in §3.1 (conducting grain with deep traps), an arriving electron is immediately moved to the accomodating trap nearest its arrival site. This nearest trap could be a vacant electron trap or an occupied hole trap; in the latter case, the charges recombine. Likewise, the hole produced in a photoemission event is immediately moved to the nearest vacant hole trap or occupied electron trap.

For model 4 in §3.1 (partially conducting grain with deep traps), each electron or hole undergoes a random walk through the grain, starting at its arrival location. In each step, the charge moves distance d_{rw} (taken to be 30 Å) in time t_{rw} . Thus, for these simulations, the time step size $dt = t_{\text{rw}}$. If a charge finds itself within distance d_{rw} of an accomodating deep trap, then it enters the trap and remains there until recombining when a charge with opposite sign arrives at the trap. The time t_{rw} is selected as follows:

$$t_{\text{rw}} = \frac{f\tau_c d_{\text{rw}}^2}{V_t^{2/3}} \quad (59)$$

with τ_c the typical time between charging events. With this choice, the typical time for a charge to travel from one trap to another is $\sim f\tau_c$. With $f \sim 1$, this model lies between the extremes of a perfect insulator and a perfect conductor with deep traps.

5 RESULTS

We ran simulations for 11 different sets of input, with 2 realizations apiece (i.e., 2 different values of the random number seed), for a total of 22 simulations. Table 1 displays input parameters for each run, as well as selected output parameters. We performed runs with models 1 through 3 of §3.1 for grain radii $a = 0.1$ and $0.2 \mu\text{m}$. For model 4, only $a = 0.1 \mu\text{m}$ is included, since the CPU time becomes prohibitive for $a = 0.2 \mu\text{m}$ when charges execute random walks through the grain volume. For models 1 through 3, the total duration of the simulation is $t_{\text{tot}} = 10^5$ yr, but substantially shorter t_{tot} were obtained for model 4.

Fig. 5 displays the component of the electric dipole moment lying along the spin axis, p_z , from a simulation for

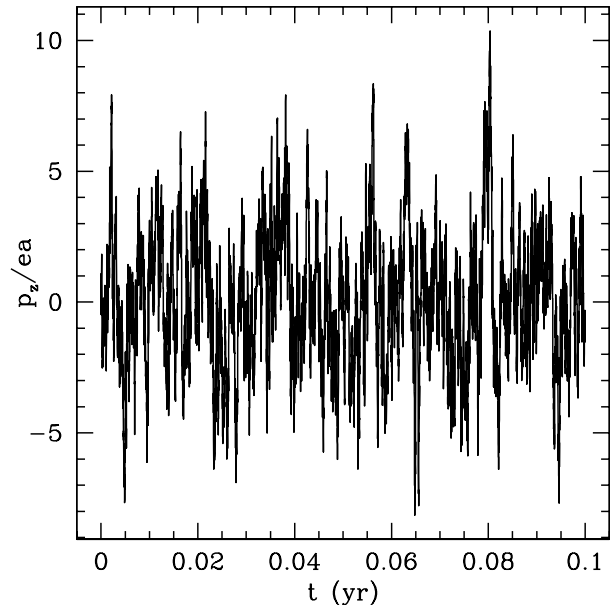


Figure 5. The component of the grain dipole moment (normalized to ea , the proton charge times the grain radius) lying along the spin axis vs. time, from a simulation of a purely insulating grain with $a = 0.1 \mu\text{m}$.

a purely insulating grain with $a = 0.1 \mu\text{m}$. Clearly, p_z reverses sign on a short time-scale of a fraction of a year. We estimate that the dipole flipping time-scale $\tau_{\text{flip}} \approx t_{\text{tot}}/N_{\text{flip}}$, where N_{flip} is the total number of dipole flips that occur in the simulation. We take a flip to occur each time $|p_z|$ increases beyond unity with p_z having the opposite sign as it did the previous time $|p_z|$ increased past unity. As seen in Table 1, $\tau_{\text{flip}} < 10^{-3}$ yr for all simulations.

The precession time $|\Omega_0|^{-1} \approx 2.7 \times 10^{-3}$ yr (1.1×10^{-2} yr) for grains with $a = 0.1 \mu\text{m}$ ($0.2 \mu\text{m}$). Thus, it is always the case that $\tau_{\text{flip}} < |\Omega_0|^{-1}$ (though not always that $\tau_{\text{flip}} \ll |\Omega_0|^{-1}$). This suggests that equation (7), i.e. $\tau_{\text{dis}} \sim \Upsilon^{-2} |\Omega_0|^{-2} \tau_{\text{flip}}^{-1}$, may be a good approximation for the disalignment time τ_{dis} . Since $\Upsilon \propto \omega^{-1}$ (eqs. 2 and 4), $\tau_{\text{dis}} \propto (\omega/\omega_T)^2$. (When $\Upsilon \ll 1$, as it is for suprathermally rotating silicate grains, $\tau_{\text{dis}} \propto \Upsilon^{-2} \propto \omega^2$ when $\tau_{\text{flip}} \gg |\Omega_0|^{-1}$ as well; eq. 8.) As a result, extremely long simulation times are needed to estimate τ_{dis} for suprathermally rotating grains. However, this proportionality also suggests a strategy for obtaining useful information with shorter simulations. We run for several values of ω/ω_T , as low as 0.1, and check the scaling of τ_{dis} versus ω/ω_T . In fact, we find that usually $\tau_{\text{dis}} \propto (\omega/\omega_T)^2$; thus, τ_{dis} for highly suprathermally rotating grains can be estimated by extrapolation. Note, also, that $\Upsilon^{-2} |\Omega_0|^{-2}$ is independent of the magnetic dipole moment μ , and hence is independent of χ_0 . Consequently, τ_{dis} does not depend on this highly uncertain parameter in this regime.

To estimate τ_{dis} from a simulation, we keep track of N_{dev} , the number of times that θ_{align} suffers a deviation of 1 rad. Once θ_{align} reaches a value $\theta_{\text{align},1}$ differing by 1 rad from its initial value, $N_{\text{dev}} = 1$. When it reaches a value differing by 1 rad from $\theta_{\text{align},1}$, $N_{\text{dev}} = 2$, etc. When $N_{\text{dev}} \gg 1$, $\tau_{\text{dis}} \approx t_{\text{tot}}/N_{\text{dev}}$. For the relatively small values of ω/ω_T under consideration, this condition obtains. However, this

Table 1. Simulation Parameters and Outputs

Model ^b	a^c μm	V_t^d \AA^3	t_{rw}^e s	Run	$ p_z _{\text{av}}^f$ ea	τ_{flip}^g 10^{-4} yr	t_{tot}^h yr	N_{dev}^a		
								1.0 ⁱ	1.5 ⁱ	2.0 ⁱ
1	0.1	1	2.21	5.2	1.0E5	2348	218	30
1	0.1	2	2.18	5.2	1.0E5	2418	195	26
2	0.1	1	2.11	...	1.0E5	72	5	1
2	0.1	2	2.12	...	1.0E5	44	6	2
3	0.1	4.0E7	...	1	1.77	6.8	1.0E5	1822	179	19
3	0.1	4.0E7	...	2	1.77	6.2	1.0E5	1800	160	19
3	0.1	4.0E6	...	1	2.11	5.8	1.0E5	2451	220	26
3	0.1	4.0E6	...	2	2.13	5.8	1.0E5	2358	228	32
4	0.1	4.0E7	2.3	1	2.16	2.2	7.29E2	14	1	0
4	0.1	4.0E7	2.3	2	2.35	2.5	7.29E2	22	1	0
4	0.1	4.0E7	1.15	1	2.17	2.5	3.64E2	6	1	0
4	0.1	4.0E7	1.15	2	2.09	2.4	3.64E2	11	1	0
4	0.1	4.0E7	9.2	1	2.56	2.4	2.92E3	81	11	1
4	0.1	4.0E7	9.2	2	2.56	2.5	2.92E3	76	7	1
4	0.1	4.0E6	2.3	1	2.07	5.0	7.29E2	17	2	0
4	0.1	4.0E6	2.3	2	2.11	5.1	7.29E2	19	3	0
1	0.2	1	2.23	2.6	1.0E5	172	16	2
1	0.2	2	2.18	2.6	1.0E5	150	12	1
2	0.2	1	2.00	...	1.0E5	4	0	0
2	0.2	2	2.00	...	1.0E5	4	1	0
3	0.2	4.0E7	...	1	2.07	2.9	1.0E5	164	17	2
3	0.2	4.0E7	...	2	2.07	2.9	1.0E5	139	14	2

^a Number of 1 rad deviations in alignment angle θ_{align} .

^b From section 3.1.

^c Grain radius.

^d Volume per deep trap.

^e Duration of random walk step.

^f Average of the absolute value of the component of the electric dipole moment lying along the spin axis (normalized to ea , the product of the proton charge and the grain radius).

^g Estimate of the electric dipole moment flipping time.

^h Duration of the simulation.

ⁱ Suprathermality ω/ω_T .

is not typically the case when $\omega/\omega_T \gtrsim 10$. In general, we estimate $\tau_{\text{dis}} \approx t_{\text{tot}}/(N_{\text{dev}} + |\Delta\theta_{\text{align}}|)$, where $\Delta\theta_{\text{align}}$ is the value of θ_{align} at the end of the simulation minus its value at the last time N_{dev} was incremented (which may have been the start of the simulation, if $N_{\text{dev}} = 0$). Table 1 indicates the values of N_{dev} for $\log_{10}(\omega/\omega_T) = 1.0, 1.5$, and 2.0 . Of course, the resulting estimate of τ_{dis} is not very reliable for the cases where $N_{\text{dev}} \sim 1$.

For each simulation, we keep track of θ_{align} for 7 different values of $\log_{10}(\omega/\omega_T)$, evenly spaced between -1.0 and 2.0. Fig. 6 displays $\cos\theta_{\text{align}}$ versus time from a simulation of a perfectly insulating grain with $a = 0.1 \mu\text{m}$ and $\omega/\omega_T = 10^2$.

Fig. 7 displays τ_{dis} versus ω/ω_T for perfectly insulating grains with $a = 0.1$ and $0.2 \mu\text{m}$. For each case, τ_{dis} is taken to be its average over the 2 realizations. The solid (dashed) curves are τ_{dis} from equation (7) for $a = 0.1 \mu\text{m}$ ($0.2 \mu\text{m}$). We employ τ_{flip} and the average value of $|p_z|$ (for use in evaluating Υ) as determined from the simulation. The agreement between the measured values of τ_{dis} and those calculated with equation (7) is surprisingly good. The expectation that $\tau_{\text{dis}} \propto (\omega/\omega_T)^2$ is well confirmed.

The disalignment times found using equation (7) and

the values of τ_{flip} from the simulations are substantially shorter than those from W06 (see figs. 2 and 3 in W06); the discrepancy exceeds 2 orders of magnitude when $a = 0.1 \mu\text{m}$. Our simulations yield much larger values of $|p_z|_{\text{av}}$ than estimated by W06, and $\tau_{\text{dis}} \propto |p_z|_{\text{av}}^{-2}$. The estimate of τ_{flip} in W06 is also substantially larger than our result. When equation (7) is used ($\tau_{\text{dis}} \propto \tau_{\text{flip}}^{-1}$), this partially compensates for the difference associated with the p_z estimates. However, given the larger estimate for τ_{flip} , W06 employed equation (8) when $a = 0.1 \mu\text{m}$; in this case, τ_{dis} is larger by a factor ≈ 2 when equation (8) is used than when equation (7) is used.

Fig. 8 shows the ratio of τ_{dis} for several simulation runs to its value for the perfectly insulating case, τ_{ins} , for $a = 0.1 \mu\text{m}$. All of the simulations from Table 1 are included, except for the perfectly conducting case. The results always lie within ≈ 50 percent of unity, with somewhat greater scatter when $\omega/\omega_T > 10$; the results for these high- ω cases are not particularly reliable, since the corresponding N_{dev} are small (see Table 1). The ratio $\tau_{\text{dis}}/\tau_{\text{ins}}$ also lies within 50 percent of unity for the model 3 run for $a = 0.2 \mu\text{m}$.

Fig. 9 displays the ratio of τ_{dis} for a perfectly conducting grain, τ_{cond} , to τ_{ins} , for $a = 0.1$ and $0.2 \mu\text{m}$. We assumed

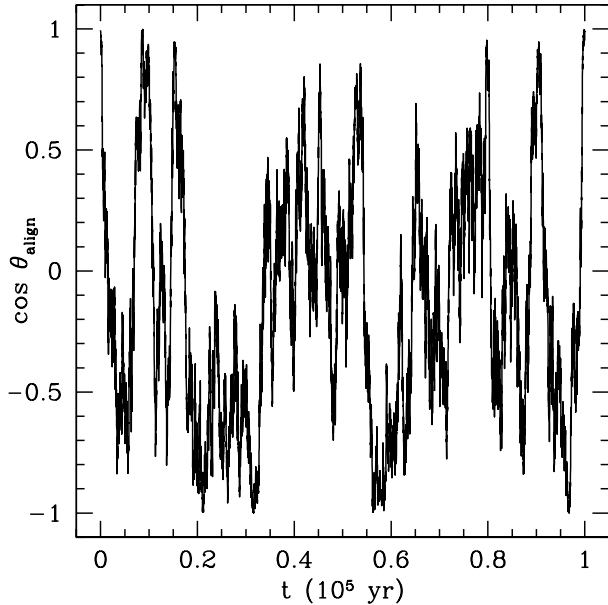


Figure 6. $\cos \theta_{\text{align}}$ versus time from a simulation of a perfectly insulating grain with $a = 0.1 \mu\text{m}$ and $\omega/\omega_T = 10^2$; $N_{\text{dev}} = 30$ for this case.

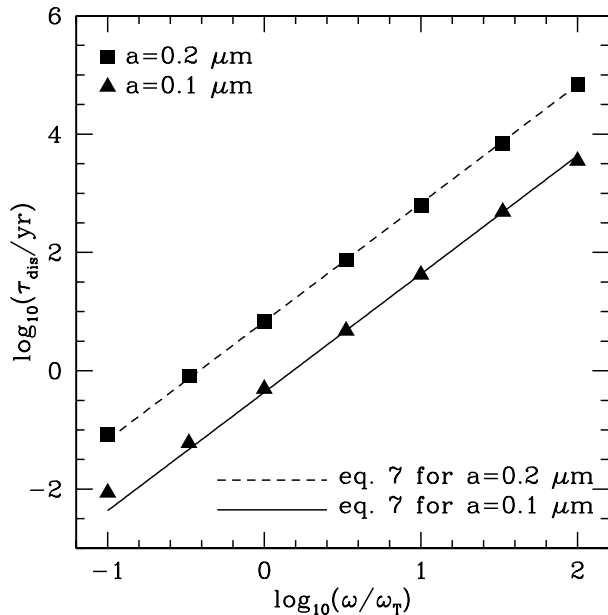


Figure 7. Disalignment time vs. suprathermality for purely insulating grains.

that $p_z = 0.1 Zea$, which seems conservative for grains sufficiently asymmetric to produce the observed polarization. However, a solution of the electrostatic boundary value problem for model aspherical grains would be needed to confirm this choice. The disalignment times tend to be 1 to 2 orders of magnitude longer for conducting grains than for insulating grains. This is not surprising, since Z , and hence p_z for conductors, does not change sign (although it does fluctuate).

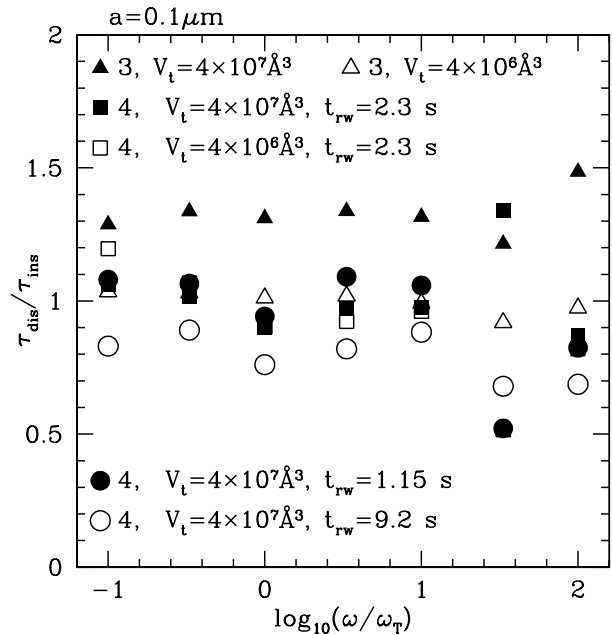


Figure 8. Ratio of disalignment time τ_{dis} for various models to that for a perfectly insulating grain, τ_{ins} , for $a = 0.1 \mu\text{m}$. Model number from §3.1; volume per deep trap, V_t ; and random walk time, t_{rw} , are indicated.

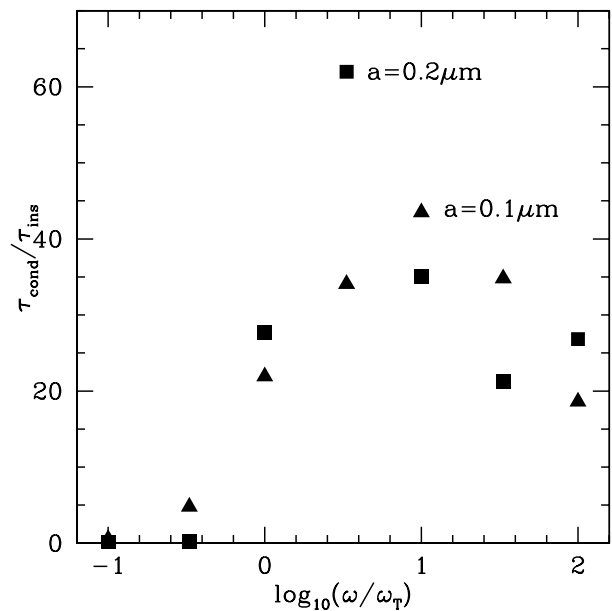


Figure 9. Ratio of disalignment time for a perfectly conducting grain, τ_{cond} , to that for a perfectly insulating grain, τ_{ins} , for $a = 0.1$ and $0.2 \mu\text{m}$, as indicated.

Note that the data points for $\omega/\omega_T \gtrsim 10$ are not reliable, given the small values of N_{dev} in these cases (Table 1).

6 CONCLUSIONS

We have conducted a more detailed analysis of grain disalignment associated with the time-varying electric dipole

moment than was attempted in W06, focusing on suprathermally rotating silicate grains. We considered 4 idealized models for how charge is transported within the grain (§3.1): a perfect insulator, 2 models involving special sites in the grain ('deep traps') where electrons or holes are effectively trapped, and a perfect conductor. The resulting disalignment times τ_{dis} for the first 3 models are highly consistent (Fig. 8) and substantially shorter (up to 2 orders of magnitude) than those obtained by W06 (cf. Fig. 7 here with figs. 2 and 3 in W06). We expect the behavior of real grains to be bracketed by these 3 models. Disalignment proceeds more slowly (up to 2 orders of magnitude; Fig. 9) for conducting grains, but we do not expect this idealization to be realistic for interstellar grains.

In treating the collisional charging, we neglected the gas-grain drift. Drift can, in principle, affect the time variation of the electric dipole moment. For a non-rotating grain, there may be a stable contribution to \mathbf{p} directed along the drift velocity. For a grain rotating uniformly about $\hat{\mathbf{a}}_1$, the charging rate may have some dependence on latitude on the grain, suppressing flips in p_z . We examine this possibility in Appendix A and conclude that flipping is not suppressed.

In the radiative torque alignment scenario, suprathermal rotation with $\omega/\omega_T \approx 100$ and alignment times $\gtrsim 10^5$ yr appear to be typical (Draine & Weingartner 1997; Lazarian & Hoang 2007; Hoang & Lazarian 2008), though additional studies are needed to confirm these results. We have found disalignment times $\lesssim 10^5$ yr when $\omega/\omega_T \approx 100$ (Figs. 7 and 8), presenting a severe challenge to the radiative torque model.

Much of the physics involved in the disalignment mechanism has not been directly verified, including the details of the charging and the turbulence-induced grain acceleration (Yan et al. 2004). Perhaps current models of these processes are incomplete in such a way as to overestimate the magnitude of the disalignment.

Alternatively, interstellar grains might contain superparamagnetic inclusions (Jones & Spitzer 1967), which could increase the magnetic susceptibility by orders of magnitude. The parameter Υ would be decreased by the same factor, and the disalignment time $\propto \Upsilon^{-2}$ when $\Upsilon \ll 1$ (eqs. 7 and 8). Recently, Lazarian & Hoang (2008) found that the presence of superparamagnetic inclusions can modify alignment by radiative torques, yielding a higher degree of alignment than experienced by grains free of inclusions. Perhaps superparamagnetic inclusions also suppress drift-induced disalignment.

ACKNOWLEDGMENTS

We are grateful to Yuri Mishin for valuable discussions and an anonymous referee for helpful comments. JCW is a Cottrell Scholar of Research Corporation.

APPENDIX A: COLLISIONAL CHARGING FOR A DRIFTING GRAIN

Consider a grain drifting with velocity \mathbf{v}_{gr} with respect to the gas. The grain rotates uniformly about $\hat{\mathbf{a}}_1$, which is inclined at angle θ_{Jv} relative to \mathbf{v}_{gr} .

To treat the collisional charging in this case, we first construct a large sphere with radius r_{big} instantaneously centered on the grain. Adopting the rest frame of the gas and taking the direction of the drift velocity \mathbf{v}_{gr} as the polar axis for spherical coordinates, the velocity \mathbf{v} of a gas-phase particle has components $(v, \theta_{\text{in}}, \phi_{\text{in}})$. The rate at which gas-phase particles enter the large sphere from within solid angle $d \cos \theta_{\text{in}} d \phi_{\text{in}}$ about $(\theta_{\text{in}}, \phi_{\text{in}})$ and with speeds between v and $v + dv$ is

$$dR = \pi r_{\text{big}}^2 n \frac{1}{4\pi} d \cos \theta_{\text{in}} d \phi_{\text{in}} P(v) dv |\mathbf{v} - \mathbf{v}_{\text{gr}}| \quad (\text{A1})$$

where $P(v)$ is the Maxwell speed distribution. After integrating over ϕ_{in} ,

$$dR = \pi r_{\text{big}}^2 n \left(\frac{8k_{\text{B}}T}{\pi m} \right)^{1/2} d\tilde{R} \quad (\text{A2})$$

with

$$d\tilde{R} = du d \cos \theta_{\text{in}} u^2 u_1 \exp(-u^2); \quad (\text{A3})$$

the dimensionless speed $u = v/v_{\text{th}}$ and

$$u_1 = (u^2 + u_{\text{gr}}^2 + 2uu_{\text{gr}} \cos \theta_{\text{in}})^{1/2} \quad (\text{A4})$$

is the particle's dimensionless speed in the rest frame of the grain ($u_{\text{gr}} = v_{\text{gr}}/v_{\text{th}}$). Integrating over the entire large sphere yields

$$\tilde{R} = 1 + \frac{u_{\text{gr}}^2}{3} - \frac{u_{\text{gr}}^4}{3} \int_0^1 dx \exp(-u_{\text{gr}}^2 x) (1 - \sqrt{x})^3. \quad (\text{A5})$$

The arrival angle θ_1 in the rest frame of the grain is characterized by

$$\cos \theta_1 = \frac{u \cos \theta_{\text{in}} + u_{\text{gr}}}{u_1}. \quad (\text{A6})$$

When $v_{\perp} = 1 \text{ km s}^{-1}$ and $T_{\text{gas}} = 100 \text{ K}$, $u_{\text{gr}} = 0.0182$ for electrons and 0.778 for protons. For each of these values of u_{gr} , we calculate u_1 and $d\tilde{R}$ for 10^{10} values of (u, θ_{in}) (10^5 for each input variable) spaced evenly in probability (as described in the text surrounding eq. 47) and with a maximum value of $u = 4$. The results are used to construct the probability $P(u_1)$ that an incoming particle has dimensionless speed in the grain's frame $\leq u_1$ (with 100 bins in u_1). For each value of u_1 , the corresponding cumulative probability $P(\cos \theta_1)$ is constructed, again with 100 bins. Note that the minimum possible value of $\cos \theta_1$ is -1 when $u > u_{\text{gr}}$ and $[1 - (u/u_{\text{gr}})^2]^{1/2}$ when $u < u_{\text{gr}}$.

To simulate the collisional charging, we adopt a time step 10 times smaller than the inverse of the rate at which electrons enter the large sphere surrounding the grain (eqs. A2 and A5). In each step, we draw a random number to determine whether or not an electron enters the large sphere; likewise for a proton. When a charged particle enters the large sphere, a value of u_1 is picked randomly from its distribution. Then, $\cos \theta_1$ is chosen randomly from the distribution for the given u_1 . The final component of the particle's velocity in the grain's rest frame, ϕ_1 , is selected randomly from a uniform distribution between 0 and 2π . Two components of the incoming particle's position remain to be determined (given $r = r_{\text{big}}$): the impact parameter b and the azimuthal angle α_1 . These are both chosen randomly (b from a uniform distribution in b^2).

At this point, the position and velocity of the incoming

particle are specified relative to a coordinate system at rest with respect to the grain and with \mathbf{v}_{gr} as the polar axis (' \mathbf{v}_{gr} -coordinates'). Denoting Cartesian axes in this coordinate system as $\hat{\mathbf{x}}_v$, $\hat{\mathbf{y}}_v$, and $\hat{\mathbf{z}}_v$, the velocity is given by

$$\mathbf{v}_1 = -v_{\text{th}}u_1(\hat{\mathbf{x}}_v \sin \theta_1 \cos \phi_1 + \hat{\mathbf{y}}_v \sin \theta_1 \sin \phi_1 + \hat{\mathbf{z}}_v \cos \theta_1) \quad (\text{A7})$$

and the position by

$$\begin{aligned} x_v &= b \cos \alpha_1 \cos \theta_1 \cos \phi_1 - b \sin \alpha_1 \sin \phi_1 \\ &\quad + z_{\text{arr}} \sin \theta_1 \cos \phi_1 \end{aligned} \quad (\text{A8})$$

$$\begin{aligned} y_v &= b \cos \alpha_1 \cos \theta_1 \sin \phi_1 + b \sin \alpha_1 \cos \phi_1 \\ &\quad + z_{\text{arr}} \sin \theta_1 \sin \phi_1 \end{aligned} \quad (\text{A9})$$

$$z_v = -b \cos \alpha_1 \sin \theta_1 + z_{\text{arr}} \cos \theta_1 \quad (\text{A10})$$

where $z_{\text{arr}} = (r_{\text{big}}^2 - b^2)^{1/2}$.

Denoting a Cartesian coordinate system attached to the grain body by (x_J, y_J, z_J) ,

$$\hat{\mathbf{z}}_J = \hat{\mathbf{a}}_1 = \hat{\mathbf{z}}_v \cos \theta_{Jv} + \hat{\mathbf{x}}_v \sin \theta_{Jv} \quad (\text{A11})$$

$$\hat{\mathbf{x}}_J = (\hat{\mathbf{x}}_v \cos \theta_{Jv} - \hat{\mathbf{z}}_v \sin \theta_{Jv}) \cos \lambda + \hat{\mathbf{y}}_v \sin \lambda \quad (\text{A12})$$

$$\hat{\mathbf{y}}_J = \hat{\mathbf{y}}_v \cos \lambda - (\hat{\mathbf{x}}_v \cos \theta_{Jv} - \hat{\mathbf{z}}_v \sin \theta_{Jv}) \sin \lambda \quad (\text{A13})$$

where λ is the phase angle of the grain's rotation and is selected randomly. (We neglect the rotation of the grain during the approach of the gas-phase particle.) Cartesian axes with \mathbf{p} as the polar axis (' \mathbf{p} -coordinates') are given by

$$\hat{\mathbf{z}}_p = \hat{\mathbf{p}} = \hat{\mathbf{x}}_J \sin \theta_{pJ} \cos \phi_{pJ} + \hat{\mathbf{y}}_J \sin \theta_{pJ} \sin \phi_{pJ} + \hat{\mathbf{z}}_J \cos \theta_{pJ} \quad (\text{A14})$$

$$\hat{\mathbf{x}}_p = \hat{\mathbf{x}}_J \cos \theta_{pJ} \cos \phi_{pJ} + \hat{\mathbf{y}}_J \cos \theta_{pJ} \sin \phi_{pJ} - \hat{\mathbf{z}}_J \sin \theta_{pJ} \quad (\text{A15})$$

$$\hat{\mathbf{y}}_p = -\hat{\mathbf{x}}_J \sin \phi_{pJ} + \hat{\mathbf{y}}_J \cos \phi_{pJ}. \quad (\text{A16})$$

From equations (A11)–(A16), we find the following dot products for use in transforming the position and velocity of the incoming gas-phase particle from \mathbf{v}_{gr} -coordinates (eqs. A7–A10) to \mathbf{p} -coordinates:

$$\hat{\mathbf{x}}_p \cdot \hat{\mathbf{x}}_v = \cos \theta_{pJ} \cos \theta_{Jv} \cos(\phi_{pJ} + \lambda) - \sin \theta_{pJ} \sin \theta_{Jv} \quad (\text{A17})$$

$$\hat{\mathbf{x}}_p \cdot \hat{\mathbf{y}}_v = \cos \theta_{pJ} \sin(\phi_{pJ} + \lambda) \quad (\text{A18})$$

$$\hat{\mathbf{x}}_p \cdot \hat{\mathbf{z}}_v = -\cos \theta_{pJ} \sin \theta_{Jv} \cos(\phi_{pJ} + \lambda) - \sin \theta_{pJ} \cos \theta_{Jv} \quad (\text{A19})$$

$$\hat{\mathbf{y}}_p \cdot \hat{\mathbf{x}}_v = -\cos \theta_{Jv} \sin(\phi_{pJ} + \lambda) \quad (\text{A20})$$

$$\hat{\mathbf{y}}_p \cdot \hat{\mathbf{y}}_v = \cos(\phi_{pJ} + \lambda) \quad (\text{A21})$$

$$\hat{\mathbf{y}}_p \cdot \hat{\mathbf{z}}_v = \sin \theta_{Jv} \sin(\phi_{pJ} + \lambda) \quad (\text{A22})$$

$$\hat{\mathbf{z}}_p \cdot \hat{\mathbf{x}}_v = \sin \theta_{pJ} \cos \theta_{Jv} \cos(\phi_{pJ} + \lambda) + \cos \theta_{pJ} \sin \theta_{Jv} \quad (\text{A23})$$

$$\hat{\mathbf{z}}_p \cdot \hat{\mathbf{y}}_v = \sin \theta_{pJ} \sin(\phi_{pJ} + \lambda) \quad (\text{A24})$$

$$\hat{\mathbf{z}}_p \cdot \hat{\mathbf{z}}_v = -\sin \theta_{pJ} \sin \theta_{Jv} \cos(\phi_{pJ} + \lambda) + \cos \theta_{pJ} \cos \theta_{Jv}. \quad (\text{A25})$$

Finally, the Cartesian \mathbf{p} -coordinates of the incoming particle's position and velocity are used in the following geometric relations to find the components in spherical coordinates:

$$r = r_{\text{big}} \quad (\text{A26})$$

$$\theta = \cos^{-1}(z_p/r) \quad (\text{A27})$$

$$\phi = 2 \tan^{-1} \left(\frac{r_{p0} - x_p}{y_p} \right) \quad (\text{A28})$$

$$\frac{dr}{dt} = \frac{1}{r} \left(x_p \frac{dx_p}{dt} + y_p \frac{dy_p}{dt} + z_p \frac{dz_p}{dt} \right) \quad (\text{A29})$$

$$\frac{d\theta}{dt} = -\frac{1}{rr_{p0}} \left(r \frac{dz_p}{dt} - z_p \frac{dr}{dt} \right) \quad (\text{A30})$$

$$\frac{d\phi}{dt} = \frac{1}{r_{p0}^2} \left(x_p \frac{dy_p}{dt} - y_p \frac{dx_p}{dt} \right) \quad (\text{A31})$$

with $r_{p0} = (x_p^2 + y_p^2)^{1/2}$. The critical impact parameter b_{crit} depends on the particle speed $v_1 = v_{\text{th}}u_1$ and $\cos \theta_0 = -v_1^{-1} dz_p/dt$ (eq. 30). If $b \leq b_{\text{crit}}$, then we integrate the equations of motion (13)–(15) to determine where on the grain surface the particle hits.

We have tried various values of r_{big} . Of course, larger values yield higher accuracy but also require smaller time steps. We found that $r_{\text{big}} = 50a$ yields high accuracy and is not prohibitively time consuming.

Substituting the collisional charging procedure described here in our charging simulations (and including both electrons and protons), we examined a perfectly insulating grain with $a = 0.1 \mu\text{m}$. With a duration of 100 yr, we found that $|p_z|_{\text{av}}/ea \approx 2.5$ and τ_{flip} ranges from 5.8×10^{-4} to 6.0×10^{-4} as $\cos \theta_{Jv}$ ranges from 0 to 1. These are very close to the results obtained previously, neglecting grain drift (and ignoring protons) in the treatment of collisional charging (see Table 1). Due to precession of \mathbf{J} about \mathbf{B} , the angle θ_{Jv} changes on a time-scale short compared with the simulation time of 100 yr (but an order of magnitude longer than τ_{flip}). However, our results imply that the behavior of the electric dipole moment is insensitive to the value of θ_{Jv} . Thus, we conclude that the neglect of grain drift in §5 does not yield significant error.

REFERENCES

- Ambegaokar V., Halperin B.I., Langer J.S., 1971, Phys. Rev. B, 4, 2612
- Blaise G., 2001, J. of Electrostatics, 50, 69
- Brucato J.R., Mennella V., Colangeli L., Rotundi A., Palumbo P., 2002, Planetary & Space Sci, 50, 829
- Dolginov A.Z., Mytrophanov I.G., 1976, Ap&SS, 43, 291
- Draine B.T., 1996, in Roberge W.G., Whittet, D.C.B., eds, ASP Conf. Ser. Vol. 97, Polarimetry of the Interstellar Medium. Astron. Soc. Pac., San Francisco, p. 16
- Draine B.T., Lazarian A., 1998, ApJ, 508, 157
- Draine B.T., Sutin B., 1987, ApJ, 320, 803
- Draine B.T., Weingartner J.C., 1997, ApJ, 480, 633
- Hoang T., Lazarian A., 2008, MNRAS, 388, 117
- Hoang T., Lazarian A., 2009, ApJ, 695, 1457
- Jones R.V., Spitzer L., 1967, ApJ, 147, 943
- Kemper F., Vriend W.J., Tielens A.G.G.M., 2004, ApJ, 609, 826 (erratum: ApJ, 633, 534)
- Kim S.-H., Martin P.G., 1995, ApJ, 444, 293
- Lazarian A., 1994, MNRAS, 268, 713
- Lazarian A., 2003, J. Quant. Spectrosc. Radiat. Transfer, 79, 881
- Lazarian A., 2007, J. Quant. Spectrosc. Radiat. Transfer, 106, 225
- Lazarian A., Draine B.T., 1997, ApJ, 487, 248
- Lazarian A., Draine B.T., 1999a, ApJ, 516, L37
- Lazarian A., Draine B.T., 1999b, ApJ, 520, L67
- Lazarian A., Hoang T., 2007, MNRAS, 378, 910
- Lazarian A., Hoang T., 2008, ApJ, 676, L25
- Lazarian A., Roberge, W.G., 1997, ApJ, 484, 230
- Li A., Draine B.T., 2001, ApJ, 550, L213

- Li M.P., Zhao G., Li A., 2007, MNRAS, 382, L26
- Mady F., Renoud R., Iacconi P., 2007, J. of Phys: Cond Matter, 19, 046219
- Martin P.G., 1971, MNRAS, 153, 279
- Martin P.G., Whittet D.C.B., 1990, ApJ, 357, 113
- Mott N.F., Davis E.A., 1971, *Electronic Processes in Non-Crystalline Materials*. Oxford University Press, Oxford
- Press W.H., Teukolsky S.A., Vetterling W.T., Flannery B.P., 1992, *Numerical Recipes in FORTRAN: The Art of Scientific Computing*, 2d ed. Cambridge Univ. Press, Cambridge
- Purcell E.M., 1975, in Field G.B., Cameron A.G.W., eds, *The Dusty Universe*. Neal Watson, New York, p. 155
- Purcell E.M., 1979, ApJ, 231, 404
- Roberge W.G., 2004, in Witt A.N., Clayton G.C., Draine B.T., eds, ASP Conf. Ser. Vol. 309, *Astrophysics of Dust*. Astron. Soc. Pac., San Francisco, p. 467
- Smith C.H., Wright C.M., Aitken D.K., Roche P.F., Hough J.H., 2000, MNRAS, 312, 327
- Spitzer L., 1941, ApJ, 93, 369
- Weingartner J.C., Draine B.T., 2001, ApJS, 134, 263 (WD01)
- Weingartner J.C., 2006, ApJ, 647, 390 (W06)
- Weingartner J.C., 2009, ApJ, 690, 875
- Whittet D.C.B., 2004, in Witt A.N., Clayton G.C., Draine B.T., eds, ASP Conf. Ser. Vol. 309, *Astrophysics of Dust*. Astron. Soc. Pac., San Francisco, p.65
- Wright C.M., Aitken D.K., Smith C.H., Roche P.F., Laureijs R.J., 2002, in Alves J., McCaughrean M., eds, *The Origins of Stars and Planets: The VLT View*. Springer-Verlag, New York, p. 85
- Yan H., Lazarian A., Draine B.T., 2004, ApJ, 616, 895